Conformational spread and dynamics in allostery of NMDA receptors

Ryan J. Durham[a,b], Nabina Paudyal[a,b], Elisa Carrillo[a], Nidhi Kaur Bhatia[a], David M. Maclean[c], Vladimir Berka[a], Drew M. Dolino[a,b], Alemayehu A. Gorfe[b,d], and Vasanthi Jayaraman[a,b,1]

[a]Center for Membrane Biology, Department of Biochemistry and Molecular Biology, University of Texas Health Science Center at Houston, Houston, TX 77030; [b]MD Anderson Cancer Center UTHealth Graduate School of Biomedical Sciences, University of Texas Health Science Center at Houston, Houston, TX 77030; [c]Department of Pharmacology and Physiology, University of Rochester Medical Center, Rochester, NY 14642; and [d]Department of Integrative Biology and Pharmacology, University of Texas Health Science Center at Houston, Houston, TX 77030

Edited by Ehud Y. Isacoff, University of California, Berkeley, CA, and approved January 6, 2020 (received for review June 25, 2019)

Allostery can be manifested as a combination of repression and activation in multidomain proteins allowing for fine tuning of regulatory mechanisms. Here we have used single molecule fluorescence resonance energy transfer (smFRET) and molecular dynamics simulations to study the mechanism of allostery underlying negative cooperativity between the two agonists glutamate and glycine in the NMDA receptor. These data show that binding of one agonist leads to conformational flexibility and an increase in conformational spread at the second agonist site. Mutational and cross-linking studies show that the dimer–dimer interface at the agonist-binding domain mediates the allostery underlying the negative cooperativity. smFRET on the transmembrane segments shows that they are tightly coupled in the unliganded and single agonist-bound form and only upon binding both agonists the transmembrane domain explores looser packing which would facilitate activation.

NMDA receptors | FRET | allostery | MD simulations

Allostery is a mechanism through which proteins are able to tune their function in response to events such as binding of ligands at regulatory sites. Initial mechanisms of allostery were based on limited conformational states of the protein leading to the classic two state and sequential models (1, 2). Given our current understanding that proteins are dynamic entities sampling an ensemble of conformations, it has become evident that the mechanism underlying allostery is based on changes in the free energy landscape brought about by a combination of changes in conformational selection and dynamics of the protein (3, 4). The measurements of conformational landscapes and dynamics have been largely limited to smaller soluble proteins due to the difficulty in using typical methods such as NMR and molecular dynamics simulations to study more complex and larger proteins such as channels, receptors, and transporters. Recent advances in single molecule fluorescence resonance energy transfer (smFRET)-based methods open the door for investigations of the dynamics and conformational landscape in larger multidomain membrane proteins (5–7), thus allowing for an understanding of allostery in these proteins in terms of these parameters.

The *N*-methyl-D-aspartate (NMDA) receptor is an ideal candidate for such a study, as the allosteric mechanism underlying the functionally well-characterized negative cooperativity between agonist binding sites, as well as activation and desensitization of the transmembrane segments, is still limited to our knowledge of the end state static structures. NMDA receptors are one of three subtypes of ionotropic glutamate receptors, which are cation-permeable ligand-gated ion channels (8–10). Glutamatergic signaling mediated by ionotropic glutamate receptors accounts for the majority of excitatory neurotransmission in the mammalian central nervous system. NMDA receptors in particular are crucial in the processes of synaptic plasticity, learning, and memory formation, as evidenced by the altered learning behavior exhibited by animals with altered NMDA receptor function and expression (11, 12). Additionally, NMDA receptors are implicated in a number of neurological disorders and diseases including ischemic stroke and epilepsy (9).

NMDA receptors are unique among the closely related glutamate receptor family members in being obligate heterotetramers consisting of glycine-binding GluN1 and glutamate-binding GluN2 subunits (13–16). Hence, the binding of both glycine and glutamate is required for receptor activation and the formation of cation-selective transmembrane channels. Endogenous glycine was initially thought to potentiate neuronal NMDA receptor currents (17) but was later established to be required for NMDA receptor activity (18). Some of the complicating factors in understanding glycine's role in NMDA receptor activation have been its high affinity to the receptor and its negative cooperativity with glutamate, which was observed as "glycine-dependent desensitization." This phenomenon, seen as an increase in "desensitization" at subsaturating concentrations of glycine, is actually deactivation that arises due to the receptor's affinity for glycine being lowered upon binding glutamate (19). This causes the initial glycine–glutamate-mediated peak current to decrease as glycine molecules dissociate from the receptor. While negative cooperativity between glutamate and glycine has been previously established through these functional measurements (20–22), the allosteric mechanism underlying the combination of repression in binding between the two agonists

Significance

NMDA receptors are the main excitatory receptors in the mammalian central nervous system. They require the binding of both glutamate and glycine for the activation of the protein. However, the binding of one agonist lowers the affinity of the second. The mechanism and physiological significance of this negative cooperativity between the two agonists is currently unknown. Using single molecule FRET and MD simulations we show that binding of one agonist destabilizes the second agonist-binding domain, making it less favorable to bind the second agonist, thus leading to lower affinity. Additionally, there is minimal effect on the transmembrane segments in the presence of a single agonist thus ensuring that the protein is activated only when bound to both agonists.

Author contributions: R.J.D., N.P., E.C., D.M.M., A.A.G., and V.J. designed research; R.J.D., N.P., E.C., N.K.B., D.M.M., V.B., and D.M.D. performed research; R.J.D., N.P., E.C., D.M.M., V.B., and V.J. analyzed data; and R.J.D., N.P., E.C., A.A.G., and V.J. wrote the paper.

The authors declare no competing interest.

This article is a PNAS Direct Submission.

[1]To whom correspondence may be addressed. Email: vasanthi.jayaraman@uth.tmc.edu.

This article contains supporting information online at https://www.pnas.org/lookup/suppl/doi:10.1073/pnas.1910950117/-/DCSupplemental.

First published February 3, 2020.

and activation of the receptor upon binding both agonists is largely unknown.

The structure of the NMDA receptor in the antagonist- and glycine–glutamate-bound states is known (13–15). NMDA receptors are modular with each subunit having distinct domains: an amino-terminal domain, an agonist-binding domain, transmembrane segments, and an intracellular C terminus. The structures, along with spectroscopic studies (5, 23, 24) and computational simulations (25, 26), show that the bilobed agonist-binding domain undergoes cleft closure upon binding agonists. The current view of activation in this receptor is hence primarily limited to these end state structures and the allosteric mechanism for activation is proposed in terms of a rigid body cleft closure conformational change being propagated to the transmembrane segments leading to receptor activation and subsequent desensitization. These structures also show two interfaces that play important roles in receptor activity (27), inhibition (28), as well as deactivation rates of agonists (29). There are currently no structures of the receptor in the presence of single agonist, hence there is currently no mechanism known, even in terms of end states, for negative cooperativity between the agonists.

Here to address the question of allostery and negative cooperativity, we have studied the conformational landscape by measuring the distance across the bilobed agonist binding clefts as well as across the transmembrane segments using smFRET. These studies are complemented with molecular dynamics (MD) simulations of the extracellular portions of one glycine-binding GluN1 and one glutamate-binding GluN2 subunit. This portion of the receptor was chosen as the minimal unit for the MD simulations due to the fact that the amino-terminal domain and agonist-binding domain of the glutamate-binding GluN2 subunit exhibit extensive interactions with the glycine-binding GluN1 agonist-binding domain. MD simulations of the ABD dimer were also performed to understand the contribution of the intradimer interface to the negative cooperativity. The combined smFRET and MD simulations are able to provide insight into the mechanism of allostery for both negative cooperativity and activation in terms of conformational fluctuations and conformational selection in this protein.

Results

Negative Cooperativity between Glycine and Glutamate. We estimated the rate of glycine dissociation in the absence of glutamate and the deactivation in the presence of glutamate by using a fast piezo-driven triple jump method on outside-out patches of HEK 293T cells expressing wild-type (WT) GluN1/GluN2A receptors. To study the deactivation of glycine in the presence of glutamate, channels were preincubated with glycine (100 μM) and then jumped into both glycine (1 mM) and glutamate (1 mM) solution for 2 to 5 ms to activate the receptors before a final jump into 5-methyl-indole 2-carboxylic acid (MeICA, 10 mM) and glutamate (1 mM) (Fig. 1*A*). MeICA is a low-affinity glycine site antagonist which prevents contaminating glycine from rebinding during this wash phase but falls off sufficiently quickly to enable rapid activation of NMDA receptors (30). To study the dissociation of glycine in the absence of glutamate, the receptors were preequilibrated with glycine (100 μM) and then jumped into a "no agonist" solution (containing MeICA, 10 mM) for variable times before a test pulse of saturating (1 mM) glutamate to probe the active fraction of channels, i.e., channels still bound to glycine (Fig. 1*B*). Using these protocols we found that the dissociation of glycine in the absence of glutamate occurred with a weighted time constant of 400 ± 50 ms ($n = 5$) while the deactivation in response to glycine removal in the presence of glutamate occurred with a weighted time constant of 119 ± 7 ms ($n = 7$, Fig. 1*C*), more than 3 times faster. Complementary experiments performed to measure the dissociation of glutamate in the presence and absence of glycine (Fig. 1 *D–F*), showed that glycine similarly increases the rate of dissociation of glutamate from 90 ± 5 ms ($n = 5$) to 50 ± 7 ms ($n = 5$), making it 1.8 times faster. These experiments establish the negative cooperativity between the ligands.

Conformational Landscape of the Agonist-Binding Domain. In order to measure conformational changes across the cleft of the glycine-binding bilobed GluN1 agonist-binding domain we introduced cysteines at sites T701 and S507 on a cys-light background GluN1 construct (Fig. 2) (GluN1*-ABD), and coexpressed it with a cys-light glutamate-binding GluN2A (GluN2A*). To measure

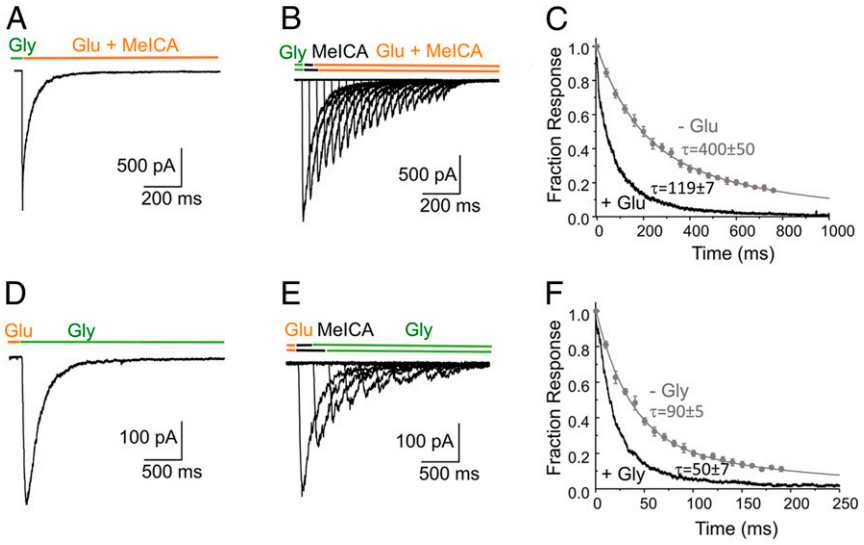

Fig. 1. Responses from outside-out patches expressing GluN1/GluN2A subunits. (*A*) Patch was equilibrated in glycine (100 μM) and jumped into glycine plus glutamate (1 mM) for 4 ms followed by glutamate and the low-affinity GluN1 competitive antagonist MeICA (10 mM) to measure receptor deactivation time course upon glycine removal in the presence of glutamate. (*B*) Patches were equilibrated with glycine before jumps of variable time into control solution with MeICA to allow for glycine dissociation followed by test pulses with glutamate. (*C*) Summary across 5 to 7 patches from experiments in *A* and *B*. (*D–F*) Complementary experiments with the roles of glycine and glutamate reversed in order to measure receptor deactivation upon glutamate removal in the presence and absence of glycine.

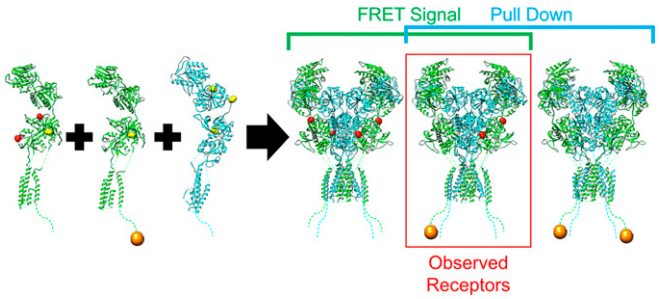

Fig. 2. Fluorescent labeling strategy for GluN1-ABD measurements. GluN1*-ABD (green, *Left*), GluN1*-streptag (green, *Middle*), and GluN2A* (cyan, *Right*) constructs were transfected into HEK 293T cells to yield the three possible subunit combinations shown on the right. Cysteines for the attachment of fluorophores are shown in red, native cysteines that were mutated to serines to prevent off-target labeling are shown in yellow, and the Twin-Strep tags used to attach the receptors to the coverslip are shown in orange. Receptors require at least one pair of fluorophores to yield a FRET signal and at least one Twin-Strep tag to attach to the coverslip; only the receptors that have both will be observed during the experiment. Structures are based on PDB: 6MMG (28).

the changes across the cleft of the glutamate-binding GluN2 agonist-binding domain we introduced cysteines at site Q503 and M701 on GluN2A* (GluN2*-ABD) and this was coexpressed with GluN1*. The functionality of the receptors was verified using electrophysiology (*SI Appendix*, Fig. S1 *A–D*), and glutamate dose–response curves were measured for the receptors to ensure that their glutamate sensitivity was not significantly different from that of wild-type receptors (*SI Appendix*, Fig. S2). In the case of GluN1*-ABD, to ensure no cross-talk across two GluN1 subunits, we coexpressed GluN1*-streptag, GluN1*-ABD, and GluN2A* subunits in HEK 293T cells, labeled them with donor and acceptor fluorophores (Alexa 555 and Alexa 647), and used in situ streptavidin pull down to attach the detergent-solubilized receptor to the streptavidin-coated coverslip (Fig. 2). This ensured only one GluN1*-ABD per receptor. GluN2*-ABD sites are such that the distances are outside significant FRET across the subunits and hence do not require this additional step. The distances within one ABD are between 33 and 40 Å which would yield FRET signal of 81 to 93%, while the shortest distance between two fluorophore attachment sites that are not on the same ABD is 65 Å, which would yield a FRET signal below 20% which is easily separated from the FRET signal of interest (28). To ensure a single FRET distance was being measured, only traces showing a single donor and single acceptor photobleaching step with anticorrelation were used. See *SI Appendix*, Fig. S3 which shows examples of single-molecule traces of donor intensity, acceptor intensity, and corresponding FRET efficiency, calculated from the donor and acceptor intensities. Efficiency traces from at least 30 molecules were used to generate ensemble-averaged FRET efficiency histograms for the GluN1 and GluN2A agonist-binding domain under conditions of apo, glycine bound, glutamate bound, and glutamate–glycine bound (Fig. 3). Wavelet-based denoising along with step transition and state identification (STaSI) analysis was used to determine the states of the receptors within the averaged FRET histogram (31, 32). Additionally, the raw

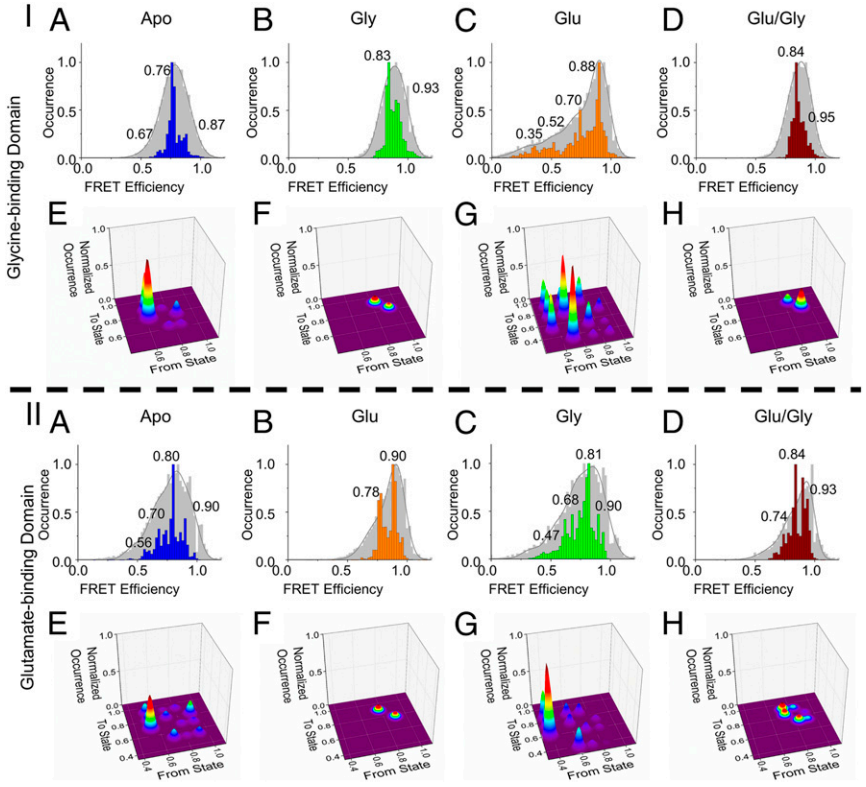

Fig. 3. smFRET histograms (*A–D*) and state transition probability maps (*E–H*) for the (I) glycine-binding domain and (II) glutamate-binding domain of the NMDA receptor. smFRET data of the GluN1*-ABD/GluN2A* receptor or the GluN1*-streptag/GluN2A*-ABD receptor was used to generate smFRET efficiency histograms. The observed histograms are shown in gray and the denoised histograms are shown in color. Individual states identified by STaSI analysis are labeled according to their efficiencies. The observed histograms were fit to Gaussian curves, and the cumulative Gaussian fit is shown as a gray curve. Additionally, the state transition probability maps for each condition are shown. A total of 1 mM glutamate and/or glycine was used as needed for the various conditions studied. Conditions shown in *I* are apo (*A* and *E*), glycine-bound (*B* and *F*), glutamate-bound (*C* and *G*), and glutamate-glycine-bound (*D* and *H*). Conditions shown in panel II are apo (*A* and *E*), glutamate-bound (*B* and *F*), glycine-bound (*C* and *G*), and glutamate-glycine-bound (*D* and *H*).

observed histograms that had not been subjected to denoising were fit to a series of Gaussian curves, and the two methods of analysis show similar states ensuring no bias from the type of analysis (*SI Appendix*, Tables S1 and S2).

Direct Effect of Agonist Binding on the Agonist-Binding Domain. The smFRET histograms for both the glycine- and glutamate-binding domains show a shift from lower to higher FRET efficiency upon agonist binding to the domain being probed (Fig. 3). The distance of 42 Å for the primary FRET efficiency state of 0.76 ± 0.01, under apo conditions in the glycine-binding domain is similar to the distance of 40 Å observed in the X-ray structure of the antagonist-bound form of this domain (33). The distance of 30 Å for the highest occupancy FRET state which has an FRET efficiency of 0.94 ± 0.05 in the glycine-bound state, is similar to 33- to 34-Å distances observed in the glycine-bound structures (33). The distance of 39 Å for the primary FRET efficiency state of 0.83 ± 0.01, under apo conditions in the glutamate-binding domain is similar to the distance of 39 Å observed in the X-ray structure of the antagonist-bound form of this domain (33). The distance of 34 Å for the primary FRET efficiency state of 0.92 ± 0.01 in the glutamate-bound state is similar to the distance of 36 Å observed in the glutamate-bound structures (33). The shift to higher FRET efficiency states indicates a shift toward shorter distances, which in turn is consistent with the prior structures and spectroscopic investigations which show a cleft closure upon binding agonists (5, 13–15, 23, 24, 34). In addition to the shift in the population, the smFRET data also show the existence of both high and low FRET states in both the apo and agonist-bound forms, albeit with differing fractions, providing direct evidence for a shift in conformation upon agonist binding toward preexisting states, which indicates a conformational selection model for agonist binding at both the glycine and glutamate site of the receptor.

To study conformational dynamics, the transition probabilities between the states were determined. The transition probability is calculated based on the number of transitions observed in the smFRET data taking into account the relative occurrence of the starting state from the smFRET traces. The transition probability maps for each measurement site were also normalized to the maximum probability observed for a given site thus allowing for comparison between different liganded conditions at a given site as well as across different sites. The normalized state transition probability maps reveal that the probabilities for the state transitions are significantly higher in the apo state (Fig. 3 I*E* and II*E*) compared to when the domain has an agonist bound to it (Fig. 3 I*F* and II*F*), showing that the conformational fluctuations are lowered when the domain is bound to an agonist.

Allosteric Effect of Second Agonist on the First Agonist-Binding Domain. The smFRET histogram for the glycine-binding domain in the presence of glutamate alone has a broad spread of FRET efficiencies (Fig. 3 I*C* and *SI Appendix*, Table S1). This condition shows population of states that are both lower and higher FRET than those observed in the apo state. This suggests that glutamate binding to the GluN2 subunit destabilizes the GluN1 glycine-binding cleft with larger conformational fluctuations. Similarly, the smFRET histogram for the glycine-binding domain in the presence of both glutamate and glycine again favors the lower 0.84 FRET efficiency (Fig. 3 I*D*) state relative to what is observed in glycine alone, suggesting that the slightly more open cleft is favored in the presence of glutamate relative to its absence even when glycine is bound. In addition to the conformational spread, the transition probabilities between states at the glycine-binding domain are significantly larger when only glutamate is bound to the receptor relative to those under apo conditions (Fig. 3 I*G* versus Fig. 3 I*E*) and are slightly higher in the glutamate–glycine-bound state relative to the glycine-alone bound state (Fig. 3 I*H* versus Fig. 3 I*F*). These results show that conformational spread favors more open cleft states and that the higher fluctuations in the conformational states allow for the receptor to transition into these open cleft states more often; these in turn are expected to favor glycine dissociation and disfavor glycine binding, thus leading to the lower affinity for glycine in the presence of glutamate.

The conformational spread at the glutamate agonist-binding site shows similar shifts as observed at the glycine agonist-binding domain. The smFRET histograms show a slight shift in population toward lower efficiencies due to the presence of glycine in both the apo state (Fig. 3 II *A* and *C*), and the glutamate-bound state (Fig. 3 II *B* and *D*). The state transition probability maps show significantly larger dynamics in the glycine-alone bound state, specifically in the transitions populating the lower FRET efficiency open cleft states (Fig. 3 II *E*–*H*). Both the shift toward lower efficiency states as well as the high probability of transitions to and from these states would contribute toward dissociation of glutamate in the presence of glycine. The differences are not as large as those observed at the glycine-binding site, which is consistent with the fact that the coagonist-induced changes in glutamate dissociation rates are smaller (1.8 times) relative to the changes in glycine dissociation (3 times).

Role of Agonist-Binding Domain Interfaces in Mediating Negative Cooperativity. The GluN1/GluN2 agonist-binding domains have two major interfaces, which are shown in Fig. 4 I*A* (interface I) and Fig. 4 II*A* (interface II). To determine the role of specific interfaces in the changes in the cleft of the individual domains and their possible role in negative cooperativity, we performed molecular dynamics simulations using minimal constructs that maintained the interfaces of interest (Fig. 4 I*A* and II*A*). To examine the cleft opening/closing dynamics, the distance histograms between the Cα atoms of T701 and S507 of the glycine-binding cleft and Q503 and M701 of the glutamate-binding cleft (which are the sites used for smFRET measurements and are shown in Fig. 4 I*A* and II*A*) were determined from the simulations after the protein was equilibrated (Fig. 4 I *B* and *C* and II *B*

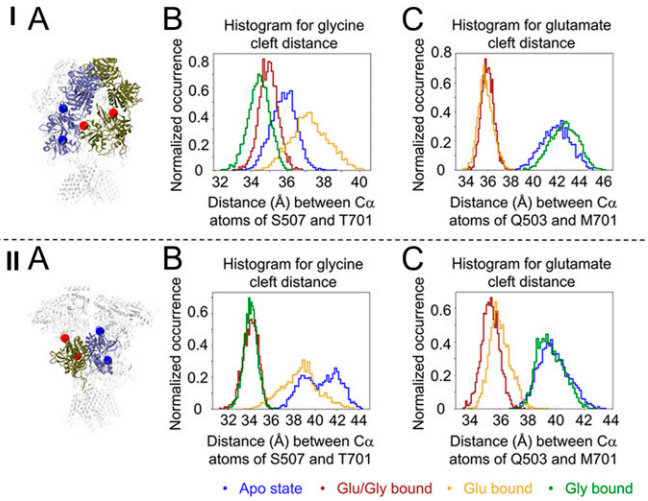

Fig. 4. Molecular dynamics measurements of the agonist-binding domains of the NMDA receptor. (I*A* and II*A*) The minimal constructs used for the simulations with GluN1 (tan), GluN2A (blue), and the residues for measuring cross-cleft distances (red and blue spheres). (I*B* and II*B*) MD measurements of the glycine-binding GluN1 cleft. The distance between Cα atoms of residues Ser-507 and Thr-701 was measured. (I*C* and II*C*) MD measurements of the glutamate-binding GluN2A cleft. The distance between Cα atoms of residues Gln-503 and Met-701 was measured.

and *C*). The glycine-binding cleft for the minimal model with interface I (Fig. 4 I*B*) shows the glycine-alone bound state to be the most closed, followed by glutamate–glycine bound, apo, and glutamate bound in that order. Similarly for the glutamate cleft for the minimal model with interface I (Fig. 4 I*C*) the most closed state is when glutamate is bound, followed by glutamate-glycine bound, apo, and glycine bound in that order. The trends observed in the MD simulations, particularly with respect to the cleft opening more in the second agonist-binding site when agonist is bound to the first site, are similar to what is observed in the experimental smFRET measurements.

The cleft histograms for simulations with the minimal model for interface II (Fig. 4 II) show no changes in the degree of cleft closure at the glycine-binding domain between the glycine-alone and glutamate–glycine bound states (Fig. 4 II*B*). The only effect seen is a shift toward a slightly more closed state at the glycine cleft when glutamate alone is bound relative to the apo state. At the cleft of the glutamate-binding domain (Fig. 4 II*C*) the cleft is open and similar in the case of glycine-alone and apo conditions. The only effect seen is again in the glutamate-alone bound state, which shows a slight opening of the glutamate-bound cleft relative to the glutamate–glycine bound state. The slightly more closed cleft state at the glycine agonist-binding domain and a slightly more open cleft at the glutamate agonist-binding domain in the presence of glutamate alone observed in the MD simulations of interface II could contribute to these states in the smFRET histograms (Fig. 3 I*C* 0.88 state and Fig. 3 II*B* 0.78 state, respectively). However, the lack of no other changes suggests that the more open cleft states relating to the cooperativity observed in the smFRET data are most likely mediated by interface I.

Role of Interface I in Negative Cooperativity. To test the results of the MD simulations that show larger changes in the minimal construct for interface I with similar trends as the smFRET data in the full-length receptor in the different liganded states, we performed smFRET measurements on the glycine-binding domain of the receptor with GluN1 in complex with GluN2A E427G. This mutation in GluN2A is present at interface I (Fig. 5 *A*, *Inset*) and has been previously shown by Regalado et al. (21) to not exhibit cooperativity between glycine and glutamate; the glycine off rates were similar in the absence and presence of glutamate and in fact slower in both cases than that observed for wild-type receptor. The smFRET histograms (Fig. 5) show a loss of the more open cleft states of the second agonist-binding site when agonist is bound to the first site than is seen in wild-type background (compare Fig. 5*C* to Fig. 3 I*C*) confirming the role of those states in mediating negative cooperativity. Additionally, there is also a decrease in the transition probability for the single agonist glutamate-bound receptor with the apo receptor showing the highest transition probabilities. This is in contrast to what was observed in the "wild-type" protein where the second agonist-binding site showed frequent transitions when agonist was bound to the first site. This indicates that dynamics, the increase in probability of the transitions, in the second agonist site when agonist is bound to the first site can also contribute toward the negative cooperativity. Finally, a higher proportion of the more closed cleft conformations is seen in the histograms under all liganded conditions relative to wild-type background. The higher fraction of the more closed cleft conformations could be related to the slower off rates seen in this mutant protein relative to wild type (21). FRET efficiencies, distances, and relative occupancies of each conformational state exhibited by the GluN1 agonist-binding domain in complex with GluN2A E427G as identified by both STaSI and Gaussian analyses are shown in *SI Appendix*, Table S3.

We also functionally tested the role of interface I in mediating negative cooperativity by introducing a cross-link across interface I between the GluN1 and GluN2A subunits. A photoactivatable unnatural amino acid, p-benzoyl-L-phenylalanine (BZP), was introduced at site 700 on GluN1 (Fig. 6*A*), and cells expressing the modified receptors were exposed to UV light in the presence of glutamate and glycine. The cross-linking across subunits was confirmed by Western blotting (see *SI Appendix*, Fig. S4 which shows the anti-GluN1 and anti-GluN2A Western blots). The glycine off rates for the cross-linked receptor in the presence and absence of glutamate show a significant decrease in cooperativity (Fig. 6 *B–D*), with glutamate causing the glycine to dissociate from the receptor only 1.4 times faster compared to the greater than 3-fold increase seen in the wild-type receptor. Although there is a fraction of the receptors that are not cross-linked, the trend of a reduction in negative cooperativity confirms the involvement of interface I in mediating the negative cooperativity.

Conformational Landscape at the Transmembrane Segments. In order to measure the distance across the GluN1 transmembrane segments, the GluN1*-TMD/GluN2A* receptor was used (Fig. 7 I, *Inset*), and to measure the distance across GluN2 the GluN1*-streptag/GluN2A*-TMD receptor was used (Fig. 7 II, *Inset*). The functionality of the GluN1*-streptag/GluN2A*-TMD receptor construct was verified (*SI Appendix*, Fig. S1*E*) and that for GluN1*-TMD/GluN2A* has been previously reported (5). It has

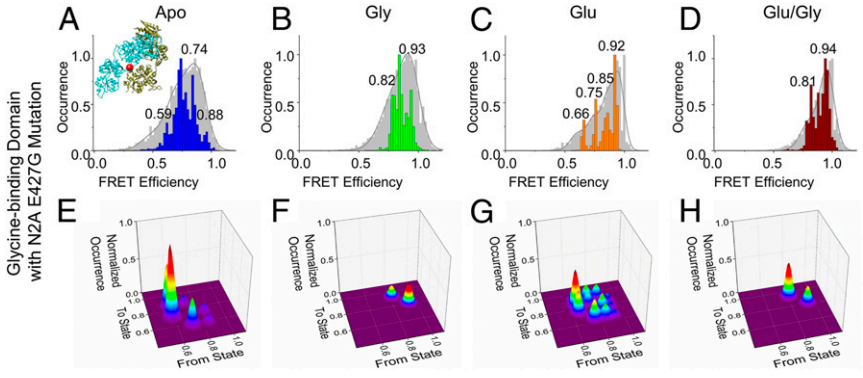

Fig. 5. smFRET histograms (*A–D*) and state transition probability maps (*E–H*) for the glycine-binding domain in the context of a GluN2A E427G mutant receptor. smFRET data of the GluN1*-ABD/GluN2A*-E427G receptor was used to generate smFRET efficiency histograms. The observed histograms are shown in gray and the denoised histograms are shown in color. Individual states identified by STaSI analysis are labeled according to their efficiencies. The observed histograms were fit to Gaussian curves, and the cumulative Gaussian fit is shown as a gray curve. Additionally, the state transition probability maps for each condition are shown. A total of 1 mM glutamate and/or glycine was used as needed for the various conditions studied. Conditions shown are apo (*A* and *E*), glycine-bound (*B* and *F*), glutamate-bound (*C* and *G*), and glutamate-glycine-bound (*D* and *H*).

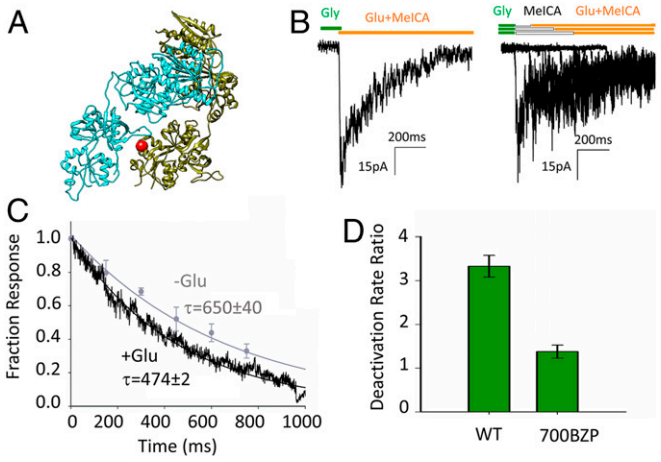

Fig. 6. Effect of interface I cross-linking on negative cooperativity. (*A*) The location of site 700 on GluN1 where the photoactivatable unnatural amino acid BZP was incorporated is shown as a red sphere in the context of interface I with GluN1 in tan and GluN2A in blue. (*B* and *C*) Measurements of the rate of glycine deactivation or dissociation in the presence or absence of glutamate using BZP cross-linked receptors. Experiments were performed using 100 μM glycine, 1 mM glutamate, and 10 nM MeICA. (*D*) The ratio of the deactivation time constants without glutamate to with glutamate for the noncross-linked receptors (WT) and the BZP cross-linked receptors (700BZP). The negative cooperativity effect of glutamate has been significantly reduced when compared to the noncross-linked receptor.

previously been shown that under resting apo conditions the smFRET histogram for the GluN1 transmembrane region is shifted toward high FRET states relative to what is observed for the glutamate-glycine-bound form of the receptor (5) (Fig. 7 I *A* and *D*). Based on the structures of the closely related Na^+/K^+ channels, for which the structures of the closed and open channel states are known (35, 36), we could conclude that the lower FRET efficiency states exhibited by the GluN1 transmembrane region could represent open or preopen channel states, which in turn is consistent with the occupancy of these low FRET states occurring only in the presence of both agonists. Here we show that addition of a single agonist glycine or glutamate (Fig. 7 I *B* and *C*) only populated the high FRET states, showing that the lower FRET open/preopen states are not populated in the presence of a single agonist. A similar trend is also observed for the smFRET measurements across the GluN2A transmembrane segments when measured at a site equivalent to that of the GluN1 transmembrane segments (Fig. 7 II). The apo state of the GluN2A transmembrane segments shows high FRET states (Fig. 7 II*A*), while the addition of glutamate with glycine caused the receptor to populate the 0.47 low FRET efficiency state that was not observed in the apo state (Fig. 7 II*D*). Binding of glutamate alone and glycine alone does not populate states below FRET efficiency of 0.5, but instead remains in states that are tightly packed (Fig. 7 II *B* and *C*). These results show that both agonists are needed to populate the lowest efficiency state. FRET efficiencies, distances, and relative occupancies of each state exhibited by the GluN1 and GluN2A transmembrane segments as identified by both STaSI and Gaussian analyses are shown in *SI Appendix*, Tables S4 and S5, respectively.

Conformational Fluctuations at the Transmembrane Segments versus Agonist-Binding Domain. The state transition probability maps for the GluN2A transmembrane domain show that the apo receptor has the lowest number of transitions, the glutamate-alone and glycine-alone bound receptors are intermediate, and the glutamate–glycine-bound receptor has the highest number of transitions (Fig. 7 II *E*–*H*). When these observations are contextualized to the changes observed in the smFRET data at the agonist-binding domain, one can see an inverse relationship between the transmembrane and agonist-binding domains emerge. Under apo conditions the GluN1 and GluN2A agonist-binding domains show large transitions (Fig. 3 I*E* and II*E*) while the transmembrane segments show very few transitons (Fig. 7 I*E* and II*E*). Additionally, the glutamate and glycine bound forms show fewer transitions at the agonist-binding domains (Fig. 3 I*H* and II*H*) but show a large number of transitions at the transmembrane domains (Fig. 7 I*H* and II*H*). Interestingly, the glutamate-alone and glycine-alone bound reeptors show that when one agonist is bound the second agonist-binding domain has a large number of transitions (Fig. 3 I *F* and *G* and II *F* and *G*); however, there are fewer transitions in the transmembrane segments (Fig. 7 I *F* and *G* and II *F* and *G*). Thus it appears that in allowing the second agonist-binding domain to be more dynamic the receptor ensures that the transmembrane segments are still tightly closed and do not populate the open channel states seen when both agonists are bound.

It should be noted that a direct comparison between the FRET-based distances and structures is not possible as the specific residue used for labeling is not resolved in the current structures, except in one glycine- and glutamate-bound structure (PBD:6IRA) where the GluN1/GluN1 distance is 36 Å (37). This is similar to the highest occupancy smFRET state, which has a distance of 40 Å.

Discussion

Historically, allostery in structured proteins has been interpreted in terms of the propagation of rigid body structural changes that are induced by agonist or effector binding. The NMDA receptor is an example of such studies where the end states have been well characterized (13–15, 34), and based on these structures the allosteric mechanism of activation has been established to be a cleft closure at the agonist-binding domains leading to motion at the transmembrane segments which results in activation. While these simplistic models are able to provide a framework for structure–function correlations, recent studies show conformational landscape and transition dynamics play essential roles in mediating allosteric communications across subunits (3, 4, 38). Here we show that negative cooperativity between glutamate and glycine as well as activation of the NMDA receptor is mediated through the intricate interplay of conformational landscape and transitions within that landscape between the different domains in this receptor. The smFRET and MD simulations presented show that the binding of an agonist at one site increases the spread of states and transitions between the states in the second agonist-binding subunit. The "destabilization" of the closed cleft state at the second site can be tied back to the lower affinity of the second agonist when the first agonist is present and thus underlies the negative cooperativity observed.

The NMDA receptors are unique among the ionotropic glutamate receptors in having an extensive interface between the GluN1 agonist-binding domain and the GluN2 amino terminal domain (Fig. 4 I*A*), in addition to the back-to-back interface of the agonist-binding domains (Fig. 4 II*A*). The role of interface II (the interface within the dimer in the agonist-binding domains of GluN1 and GluN2A) has been studied extensively, as this interface was first observed in the initial crystal structures of the isolated agonist-binding domain (29). Interface II is similar to what is observed in the AMPA and kainate receptors, and it is the site of binding of allosteric modulators and ions (39, 40). In NMDA receptors, a mutation at site Y535 in this interface has been shown to alter deactivation. Interface II is also the site of positive and negative allosteric modulators (41, 42). We hence performed MD simulations on this dimer construct to determine its contributions toward negative cooperativity. Our data show that the binding of glutamate alone causes the glycine cleft to adopt a more closed conformation relative to no ligand being

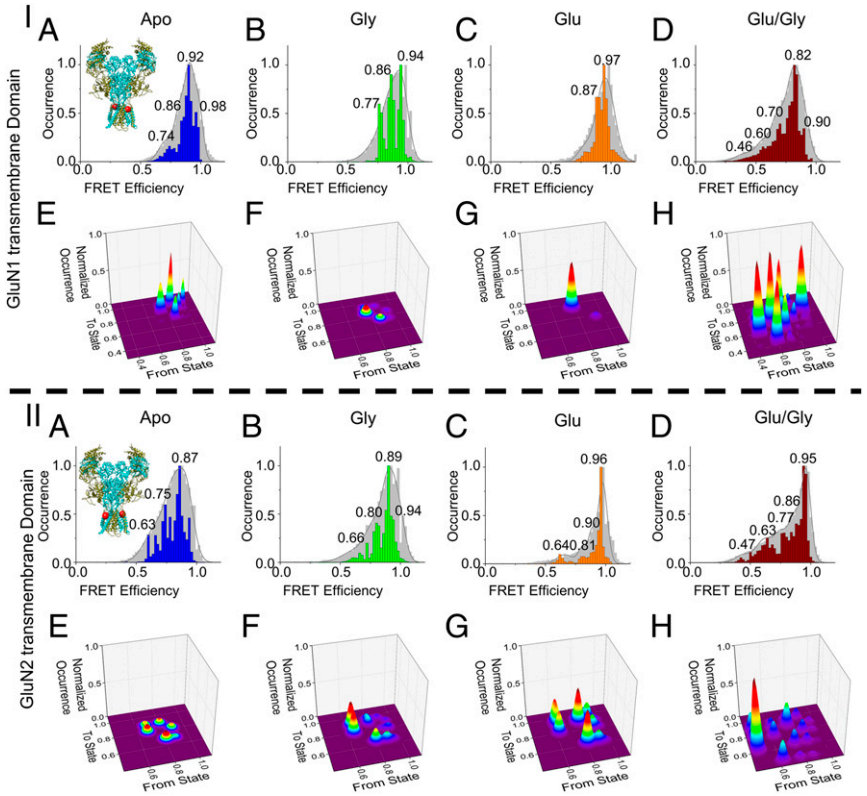

Fig. 7. smFRET histograms (*A–D*) and state transition probability maps (*E–H*) for the transmembrane region of the (I) GluN1 and (II) GluN2A subunits. smFRET data of the GluN1*-TMD/GluN2A* receptor or the GluN1*-streptag/GluN2A*-TMD receptor was obtained and used to generate smFRET efficiency histograms. The observed histograms are shown in gray and the denoised histograms are shown in color. Individual states identified by STaSI analysis are labeled according to their efficiencies. The observed histograms were fit to Gaussian curves, and the cumulative Gaussian fit is shown as a gray curve. Additionally, the state transition probability maps for each condition are shown. A total of 1 mM glutamate and/or glycine was used as needed for the various conditions studied. GluN1 apo and glu/gly data (*A*, *E*, *D*, and *H* in panel I) are from ref. 5. Conditions shown in both panels I and II are apo (*A* and *E*), glycine-bound (*B* and *F*), glutamate-bound (*C* and *G*), and glutamate-glycine-bound (*D* and *H*).

present at both domains, which would suggest a slower dissociation of glycine in the presence of glutamate and is more consistent with positive cooperativity and not negative cooperativity, counter to observations using electrophysiology and spectroscopy. MD simulations on interface I (the interdimer interface between the agonist-binding domain of GluN1 and the amino terminal and agonist-binding domains of GluN2A), on the other hand, show trends similar to what is observed in the smFRET measurements.

Previous structural and functional studies have shown the importance of interface I in mediating zinc allosteric inhibition, gating, and agonist efficacy (21, 27, 28). Specifically, Esmenjaud et al. demonstrated that the introduction of cysteine cross-links across interface I, between the agonist-binding domains of GluN1 and GluN2, can lock the receptor into an active, "rolled" conformation (27). The receptor locked into the rolled conformation also demonstrated increased EC_{50} values for both glycine and glutamate. Additionally, Regalado, et al. (21) showed that a mutation, E427G, at this interface eliminated the negative cooperativity. Here we performed smFRET measurements on this mutation and show a loss in the more open cleft state and a reduction in the higher state transition dynamics at the glycine site in the presence of glutamate. These data further confirm the role of these states and dynamics in mediating negative cooperativity. The selective loss of the more open cleft state in the E427G mutant also suggests that the more open cleft states observed at the second agonist-binding domain are not likely due to an unstable fragile state of the receptor due to sample preparation in the smFRET measurements.

The smFRET measurements at the transmembrane domain were performed to determine the changes at the functional segment of the protein due to single agonist binding. These data show tightly packed states at the pre-M1 helices of both subunits of the NMDA receptor in the presence of single agonist. It is interesting to note that the binding of glycine alone shows a higher fraction of the lower FRET efficiency state for measurements across both GluN1 and GluN2, relative to the glutamate-alone bound state. Additionally, the dynamics of the changes at the GluN1 transmembrane domain are larger in the glutamate–glycine-bound state relative to what is observed across the GluN2 subunits. Prior functional measurements have shown differences in the extent of agonist-activation coupling for glutamate and glycine and these differences seen in the smFRET measurements here may be reflective of these differences (43). Further, the absence of more loosely packed transmembrane states in the single agonist-bound state suggests that the negative cooperativity may be a mechanism to ensure that the conformational entropy loss associated with binding of a single agonist at its binding site is transmitted to the adjacent agonist-binding domain and not the transmembrane segments, thus ensuring that the receptor only opens in the presence of both agonists and emphasizing the role of allostery in fine tuning regulation.

Materials and Methods

DNA Construct Design. Wild-type *Rattus norvegicus* GluN1 and GluN2A (provided by S. Nakanishi, Osaka Bioscience Institute, Osaka, Japan) were mutated such that all extracellular nondisulfide-bonded cysteines were

changed to serines (C459 in GluN1) (C231, C399, and C460 in GluN2A). These "cys-light" constructs (GluN1* and GluN2A*) were further modified using site-directed mutagenesis to create the constructs used in the smFRET experiments. For the first construct, a C-terminal Twin-Strep tag was added to the GluN1* (GluN1*-streptag). For the second construct, T701 and S507 of the GluN1* were changed to cysteines (GluN1*-ABD). For the third construct, F553 of the GluN2A* was changed to a cysteine (GluN2A*-TMD). For the fourth construct, Q503 and M701 of the GluN2A* construct were changed to cysteines (GluN2A*-ABD). All constructs are contained in the pcDNA 3.1 vector and have been shown via electrophysiology to form functional receptors (*SI Appendix*, Fig. S1). The GluN1*-TMD construct consists of the GluN1* with F554 changed to a cysteine. This construct has been previously used and shown to be functional by electrophysiology (5). For the smFRET on the mutant GluN2A receptor, E427 of GluN2A* was changed to a glycine (GluN2A*-E427G). All mutations were verified with Sanger sequencing (Genewiz).

smFRET Data Collection and Analysis. The details for smFRET sample preparation and data acquisition are provided in *SI Appendix, SI Text*. A detailed protocol for smFRET data collection and analysis is also provided in Litwin et al. (44). For liganded conditions, 1 mM glutamate and 1 mM glycine were used, and for apo conditions at the glycine site glycine oxidase was used to remove contaminating glycine. The number of molecules included in the final analysis for each condition is as follows: GluN1 ABD apo $n = 33$, gly $n = 46$, glu $n = 38$, glu-gly $n = 32$; GluN2A ABD apo $n = 31$, gly $n = 35$, glu $n = 32$, glu-gly $n = 34$; GluN1 ABD with GluN2A E427G apo $n = 36$, gly $n = 31$, glu $n = 41$, glu-gly $n = 30$; GluN1 TMD gly $n = 43$, glu $n = 33$; GluN2A TMD apo $n = 45$, gly $n = 32$, glu $n = 40$, and glu-gly $n = 80$. Using Matlab (MathWorks), the data were subjected to wavelet denoising. FRET efficiencies were calculated using the intensity of the acceptor and the intensity of the donor. Corrections for both donor and acceptor intensity were made to subtract background and cross-talk, as well as to correct for differences in quantum yield and detector efficiency prior to calculating FRET efficiency. The resulting efficiency traces were compiled into histograms showing the relative occupancy of various FRET efficiencies. The histograms were fit to Gaussian curves to reveal the underlying conformational states using Origin software (OriginLab).

Photo Cross-Linking. In order to perform the unnatural amino acid cross-linking at interface I, an amber stop codon (tag) was introduced at site 700 of GluN1 using site-directed mutagenesis. The GluN1 700tag DNA and GluN2A WT DNA were cotransfected into HEK 293T cells along with DNA constructs encoding the aminoacyl-tRNA synthetase p-benzoyl-L-phenylalanine tRNA synthetase (BZPRS) and the tag-codon compatible tRNA. The unnatural amino acid BZP was included in the media during and after transfection at a concentration of 1 mM. These DNA constructs were transfected at a ratio of 10:3:2:10 μg GluN1:GluN2A:BZPRS:tRNA.

Cross-linking between the subunits of the BZP-containing NMDA receptor was induced via exposure of receptors to UV light. The transfected cells were washed with PBS and exposed to UV light of wavelength 254 nm using a Stratalinker 1800 at an intensity of 3 mM/cm^2 for 3 to 15 min on ice. Cross-linking was carried out in the presence of 100 μM glutamate and glycine and 5 mM $MgCl_2$. SDS/PAGE was performed on the receptors to validate the intersubunit cross-link. Anti-GluN1 antibody ab134308 (Abcam) and anti-GluN2A antibody ab240884 (Abcam) were used to probe for GluN1 and GluN2A, respectively, and observe the shift in molecular weight associated with the formation of the GluN1/GluN2A cross-linked dimer.

Electrophysiology. HEK 293T cells at 40 to 50% confluency in 35-mm dishes were transfected using Lipofectamine 2000 (Invitrogen) and cotransfected with GFP. The amounts of 300 μM (2R)-amino-5-phosphonopentanoate and 30 μM 5,7-dichlorokynurenic acid were present in the medium during and after transfection. Whole-cell patch clamp recordings were performed 24 h after transfection using fire-polished borosilicate glass pipettes (Sutter instruments) with 3- to 5-MΩ resistance and filled with internal solution (135 mM CsF, 33 mM CsOH, 2 mM $MgCl_2$, 1 mM $CaCl_2$, 11 mM EGTA, 10 mM Hepes, adjusted to pH 7.4 with CsOH). The external solution (140 mM NaCl, 2.8 mM KCl, 1 mM $CaCl_2$, 10 mM Hepes, adjusted to pH 7.4 with NaOH) was (with and without 1 mM glutamate and 1 mM glycine) applied to lifted cells using a stepper motor system (SF-77B, Warner Instruments) with triple barrel tubing. Recordings were performed using an Axopatch 200B amplifier (Molecular Devices) at −60 mV hold potential, acquired at 10 kHz using pCLAMP10 software (Molecular Devices), and filtered online at 5 kHz. Outside-out patch recordings were performed 24 to 48 h posttransfection using the same pipettes, solution composition, and amplifier (but with 50 kHz acquisition and 10 kHz filtering). Patches were positioned in front of a custom-built triple barrel perfusion tool (45), and solution exchange times using open tip currents were routinely measured at the end of each experiment (200 to 400 μs). Data from either deactivation decays or dissociation decays were fit to a double exponential decay with a fixed zero offset (Figs. 1 and 6). Patches were individually fit and the results averaged to provide the reported weighted time constants.

Homology Modeling and Molecular Dynamics Simulations. In order to perform the molecular dynamics simulations on interface I, a homology model for the dimer of a heteromeric GluN1/GluN2A NMDA receptor (Fig. 4 I*A*) was built by using MODELLER (46) software. The template structure chosen for modeling was the crystal structure of the *R. norvegicus* GluN1/GluN2B NMDA receptor (Protein Data Bank [PDB]: 4PE5) (14). The *R. norvegicus* GluN2A sequence was used to prepare the homology model and exhibited ∼72% sequence identity with GluN2B. The *R. norvegicus* sequences can be accessed in the UniProt Database with UniProt ID P35439 for GluN1, Q00959 for GluN2A, and Q00960 for GluN2B. Ten model structures were prepared, and the structure with the lowest Discrete Optimized Protein Energy (DOPE) score was utilized in the simulations. A dimer of the extracellular domain was used as the minimal construct for the simulations (Fig. 4 I*A*) in order to preserve the extensive interactions between the two subunits at interface I. Four independent simulations were performed: one bound to glycine, one bound to glutamate, one bound to both, and one bound to neither. In all simulations, missing residues and hydrogen atoms were added to the structure using the psfgen (47) module of the Visual Molecular Dynamics software (VMD) (48) and the structure was then placed at the center of a 113 × 124 × 136 Å box containing 17 to 19 charge-neutralizing sodium ions and ∼55,190 TIP3P water molecules. The total number of atoms for the simulations of interface I ranged from 186,639 to 186,666. Each system was energy minimized using 5,000 steps of conjugate gradient energy minimization applying a restraint force of spring constant 4 kcal/mol/Å^2 on the backbone atoms as well as on the sidechain heavy atoms of residues directly interacting with the ligands. This was followed by a 5-ns equilibration simulation using a 1-fs time step while progressively decreasing the restraint force constant to zero. Subsequent production runs of ∼500 ns each were conducted using a time step of 2 fs under a constant number of particles (N), pressure (P = 1 bar), and temperature (T = 310 K) ensemble, with pressure controlled by the Nose-Hoover Langevin piston and temperature by the Langevin thermostat. Periodic boundary conditions were used. Long-range electrostatic interactions were calculated by the particle mesh Ewald (PME) method (49), with covalent bonds involving hydrogen atoms restrained by SHAKE. Short-range nonbonded interactions were smoothly switched off between 10 Å and 12 Å with a 14-Å cutoff used for pair list updates. The simulations were conducted using the program NAMD 2.12 (50) and the CHARMM36 force field (51) for the NMDA receptor with the application of the cMAP dihedral correction and the CHARMM general force field (CGENFF) (52) for the ligands. Analysis was conducted using Tcl scripts and VMD (48).

In order to perform the molecular dynamics simulations on interface II (Fig. 4 II*A*), structures for the isolated agonist-binding domain dimer of GluN1/GluN2A were selected as the starting points. The structure PDB 5I57 (42) was chosen as the starting point for the glutamate–glycine-bound condition and the glutamate-only bound condition. For the glycine-only bound condition PDB 4NF5 (33) was used, and for the no ligand bound condition PDB 4NF4 (33) was used. For each simulation, missing residues and hydrogens were added to the structure as described above, and the structure was placed at the center of a 60 × 68 × 75 Å box containing 6 to 9 charge neutralizing chloride ions and 21,532 to 23,141 TIP3P water molecules. The total number of atoms for the simulations of interface II ranged from 73,301 to 78,323. Energy minimization and equilibration simulation were then carried out as described above. Subsequent production runs of ∼250 ns each were conducted using a time step of 2 fs under a constant number of particles (N), pressure (P = 1 bar), and temperature (T = 310 K) ensemble. The remainder of the simulation steps were carried out as described above.

Data and Materials Availability. All data and details about materials used are presented in the paper and *SI Appendix*.

ACKNOWLEDGMENTS. This project was supported by NIH funding F31GM130035 to R.J.D., K99NS094761 to D.M.M., R01GM124233 to A.A.G., and R35GM122528 to V.J. Additional funding support was provided by the Houston

Area Molecular Biophysics Training Program to N.P., the American Heart Association Postdoctoral Fellowship Program to E.C., the Training Interdisciplinary Pharmacology Scientists Program to D.M.D., and the Cancer Prevention and Research Institute of Texas DP150093 to A.A.G. We are grateful to the Texas Advanced Computing Center for providing us with the computer resources needed to perform the MD simulations that were included in this paper.

1. J. Monod, J. Wyman, J. P. Changeux, On the nature of allosteric transitions: A plausible model. *J. Mol. Biol.* **12**, 88–118 (1965).
2. D. E. Koshland, , Jr, G. Némethy, D. Filmer, Comparison of experimental binding data and theoretical models in proteins containing subunits. *Biochemistry* **5**, 365–385 (1966).
3. V. J. Hilser, Biochemistry. An ensemble view of allostery. *Science* **327**, 653–654 (2010).
4. D. Kern, E. R. Zuiderweg, The role of dynamics in allosteric regulation. *Curr. Opin. Struct. Biol.* **13**, 748–757 (2003).
5. D. M. Dolino *et al*., The structure-energy landscape of NMDA receptor gating. *Nat. Chem. Biol.* **13**, 1232–1238 (2017).
6. S. A. Shaikh *et al*., Stargazin modulation of AMPA receptors. *Cell Rep.* **17**, 328–335 (2016).
7. R. Vafabakhsh, J. Levitz, E. Y. Isacoff, Conformational dynamics of a class C G-protein-coupled receptor. *Nature* **524**, 497–501 (2015).
8. S. F. Traynelis *et al*., Glutamate receptor ion channels: Structure, regulation, and function. *Pharmacol. Rev.* **62**, 405–496 (2010).
9. K. B. Hansen, F. Yi, R. E. Perszyk, F. S. Menniti, S. F. Traynelis, NMDA receptors in the central nervous system. *Methods Mol. Biol.* **1677**, 1–80 (2017).
10. G. J. Iacobucci, G. K. Popescu, NMDA receptors: Linking physiological output to biophysical operation. *Nat. Rev. Neurosci.* **18**, 236–249 (2017).
11. E. Shimizu, Y. P. Tang, C. Rampon, J. Z. Tsien, NMDA receptor-dependent synaptic reinforcement as a crucial process for memory consolidation. *Science* **290**, 1170–1174 (2000).
12. S. M. Rodrigues, G. E. Schafe, J. E. LeDoux, Intra-amygdala blockade of the NR2B subunit of the NMDA receptor disrupts the acquisition but not the expression of fear conditioning. *J. Neurosci.* **21**, 6889–6896 (2001).
13. S. Zhu *et al*., Mechanism of NMDA receptor inhibition and activation. *Cell* **165**, 704–714 (2016).
14. E. Karakas, H. Furukawa, Crystal structure of a heterotetrameric NMDA receptor ion channel. *Science* **344**, 992–997 (2014).
15. N. Tajima *et al*., Activation of NMDA receptors and the mechanism of inhibition by ifenprodil. *Nature* **534**, 63–68 (2016).
16. R. E. Sirrieh, D. M. MacLean, V. Jayaraman, Amino-terminal domain tetramer organization and structural effects of zinc binding in the N-methyl-D-aspartate (NMDA) receptor. *J. Biol. Chem.* **288**, 22555–22564 (2013).
17. J. W. Johnson, P. Ascher, Glycine potentiates the NMDA response in cultured mouse brain neurons. *Nature* **325**, 529–531 (1987).
18. N. W. Kleckner, R. Dingledine, Requirement for glycine in activation of NMDA-receptors expressed in Xenopus oocytes. *Science* **241**, 835–837 (1988).
19. M. L. Mayer, L. Vyklicky, Jr, J. Clements, Regulation of NMDA receptor desensitization in mouse hippocampal neurons by glycine. *Nature* **338**, 425–427 (1989).
20. M. Benveniste, J. M. Mienville, E. Sernagor, M. L. Mayer, Concentration-jump experiments with NMDA antagonists in mouse cultured hippocampal neurons. *J. Neurophysiol.* **63**, 1373–1384 (1990).
21. M. P. Regalado, A. Villarroel, J. Lerma, Intersubunit cooperativity in the NMDA receptor. *Neuron* **32**, 1085–1096 (2001).
22. K. A. Cummings, G. K. Popescu, Glycine-dependent activation of NMDA receptors. *J. Gen. Physiol.* **145**, 513–527 (2015).
23. A. Rambhadran, J. Gonzalez, V. Jayaraman, Subunit arrangement in N-methyl-D-aspartate (NMDA) receptors. *J. Biol. Chem.* **285**, 15296–15301 (2010).
24. D. R. Cooper *et al*., Conformational transitions in the glycine-bound GluN1 NMDA receptor LBD via single-molecule FRET. *Biophys. J.* **109**, 66–75 (2015).
25. Y. Yao, J. Belcher, A. J. Berger, M. L. Mayer, A. Y. Lau, Conformational analysis of NMDA receptor GluN1, GluN2, and GluN3 ligand-binding domains reveals subtype-specific characteristics. *Structure* **21**, 1788–1799 (2013).
26. A. Yu *et al*., Molecular lock regulates binding of glycine to a primitive NMDA receptor. *Proc. Natl. Acad. Sci. U.S.A.* **113**, E6786–E6795 (2016).
27. J. B. Esmenjaud *et al*., An inter-dimer allosteric switch controls NMDA receptor activity. *EMBO J.* **38**, e99894 (2019).
28. F. Jalali-Yazdi, S. Chowdhury, C. Yoshioka, E. Gouaux, Mechanisms for zinc and proton inhibition of the GluN1/GluN2A NMDA receptor. *Cell* **175**, 1520–1532.e15 (2018).
29. H. Furukawa, S. K. Singh, R. Mancusso, E. Gouaux, Subunit arrangement and function in NMDA receptors. *Nature* **438**, 185–192 (2005).
30. R. Nahum-Levy, D. Lipinski, S. Shavit, M. Benveniste, Desensitization of NMDA receptor channels is modulated by glutamate agonists. *Biophys. J.* **80**, 2152–2166 (2001).
31. B. Shuang *et al*., Fast step transition and state identification (STaSI) for discrete single-molecule data analysis. *J. Phys. Chem. Lett.* **5**, 3157–3161 (2014).
32. D. M. Dolino *et al*., Structural dynamics of the glycine-binding domain of the N-methyl-D-aspartate receptor. *J. Biol. Chem.* **290**, 797–804 (2015).
33. A. Jespersen, N. Tajima, G. Fernandez-Cuervo, E. C. Garnier-Amblard, H. Furukawa, Structural insights into competitive antagonism in NMDA receptors. *Neuron* **81**, 366–378 (2014).
34. C. H. Lee *et al*., NMDA receptor structures reveal subunit arrangement and pore architecture. *Nature* **511**, 191–197 (2014).
35. A. Alam, Y. Jiang, High-resolution structure of the open NaK channel. *Nat. Struct. Mol. Biol.* **16**, 30–34 (2009).
36. N. Shi, S. Ye, A. Alam, L. Chen, Y. Jiang, Atomic structure of a Na+- and K+-conducting channel. *Nature* **440**, 570–574 (2006).
37. J. B. Zhang *et al*., Structural basis of the proton sensitivity of human GluN1-GluN2A NMDA receptors. *Cell Rep.* **25**, 3582–3590.e4 (2018).
38. S. Kim *et al*., Probing allostery through DNA. *Science* **339**, 816–819 (2013).
39. A. J. Plested, R. Vijayan, P. C. Biggin, M. L. Mayer, Molecular basis of kainate receptor modulation by sodium. *Neuron* **58**, 720–735 (2008).
40. Y. Sun *et al*., Mechanism of glutamate receptor desensitization. *Nature* **417**, 245–253 (2002).
41. D. H. Hackos *et al*., Positive allosteric modulators of GluN2A-containing NMDARs with distinct modes of action and impacts on circuit function. *Neuron* **89**, 983–999 (2016).
42. F. Yi *et al*., Structural basis for negative allosteric modulation of GluN2A-containing NMDA receptors. *Neuron* **91**, 1316–1329 (2016).
43. R. Kazi, J. Dai, C. Sweeney, H. X. Zhou, L. P. Wollmuth, Mechanical coupling maintains the fidelity of NMDA receptor-mediated currents. *Nat. Neurosci.* **17**, 914–922 (2014).
44. D. B. Litwin, R. J. Durham, V. Jayaraman, Single-molecule FRET methods to study glutamate receptors. *Methods Mol. Biol.* **1941**, 3–16 (2019).
45. D. M. MacLean, S. S. Ramaswamy, M. Du, J. R. Howe, V. Jayaraman, Stargazin promotes closure of the AMPA receptor ligand-binding domain. *J. Gen. Physiol.* **144**, 503–512 (2014).
46. B. Webb, A. Sali, Comparative protein structure modeling using MODELLER. *Curr. Protoc. Bioinf.* **86**, 2.9.1–2.9.37 (2016).
47. J. Gullingsrud, C. Kim, S. S. Taylor, J. A. McCammon, Dynamic binding of PKA regulatory subunit RI alpha. *Structure* **14**, 141–149 (2006).
48. W. Humphrey, A. Dalke, K. Schulten, VMD: Visual molecular dynamics. *J. Mol. Graphics* **14**, 33–38 (1996).
49. T. Darden, D. York, L. Pedersen, Particle mesh Ewald: An N· log (N) method for Ewald sums in large systems. *J. Chem. Phys.* **98**, 10089–10092 (1993).
50. J. C. Phillips *et al*., Scalable molecular dynamics with NAMD. *J. Comput. Chem.* **26**, 1781–1802 (2005).
51. R. B. Best *et al*., Optimization of the additive CHARMM all-atom protein force field targeting improved sampling of the backbone φ, ψ and side-chain χ(1) and χ(2) dihedral angles. *J. Chem. Theory Comput.* **8**, 3257–3273 (2012).
52. K. Vanommeslaeghe *et al*., CHARMM general force field: A force field for drug-like molecules compatible with the CHARMM all-atom additive biological force fields. *J. Comput. Chem.* **31**, 671–690 (2010).